MSEC2014-3930

ENHANCED SURFACE RESIDUAL COMPRESSION OF CARBURIZED STEEL PARTS USING LASER PEENING PROCESS WITH PRELOAD

Zhichao (Charlie) Li, PhD, and B. Lynn Ferguson, PhD
DANTE Solutions, Inc.
7261 Engle Road, Suite 105
Cleveland, Ohio, USA
Charlie.Li@Dante-Solutions.com

KEYWORDS

Laser Peening, Carburization, Quench Hardening, Phase Transformation, Computer Modeling, Residual Stress, Bending Fatigue

ABSTRACT

Residual stresses are critical to the fatigue performance of parts. In general, compressive residual stress in the surface is beneficial, and residual tension is detrimental because of the effect of stress on crack initiation and propagation. Carburization and quench hardening create compressive residual stresses in the surface of steel parts. The laser peening process has been successfully used to introduce residual compression to the surface of nonferrous alloy parts. However, the application on carburized steel parts has not been successful so far. The application of laser peening on carburized steel parts is limited due to two main reasons: 1) the high strength and low ductility of carburized case, and 2) the compressive residual stresses in the surface of the part prior to laser peening. In this paper, the carburization, quench hardening, and laser peening processes are integrated using finite element modeling. The predicted residual stresses from quench hardening and laser peening are validated against residual stresses determined from X-ray diffraction measurements. An innovative concept of laser peening with preload has been invented to enhance the residual compression in a specific region of laser peened parts. This concept is proved by FEA models using DANTE-LP.

INTRODUCTION

Laser peening has been successfully used to introduce compressive residual stresses in critical regions of many nonferrous components [1-3]. It is well known that residual surface compression at critical locations benefits fatigue performance because the compression postpones the initiation and propagation of cracks [4-6]. In general, higher magnitude and a greater depth of the compressive surface layer are preferred. The residual stresses introduced by a laser peening process are highly dependent on the part geometry, laser intensity, pulse duration, power distribution, spot size, peening sequence, and the ablative layer material and thickness. For example, higher laser intensity and longer pulse tend to drive the residual compression deeper. However, the higher intensity also leads to a higher degree of stress variation from spot to spot due to the peening sequential effect. Most laser peening applications on nonferrous alloy components start with neutral or tensile stresses at the surface. Experience has shown that laser peening part surfaces with neutral or tensile residual stresses effectively produces residual compressive stresses. Many steel components are carburized and then hardened using quenching processes. The carburization and quenching create compressive residual stresses in the surface of these components. The effect of residual compression prior to laser peening has been studied using both modeling and experiments, and the response is different.

Thermal gradients, phase transformations, and stress interact with each other during quench hardening process of steel components [7-8]. Finite element modeling has been successfully used to predict the material properties, hardness, residual stresses and distortion using DANTE [9-12]. Figure 1 shows schematically the required input, material models, and output for modeling the heat treatment process of steel components. DANTE-LP is a set of user subroutines that link with ABAQUS/Standard and ABAQUS/Explicit to model the laser peening process. A modified Johnson-Cook model is used to describe the high strain rate material behavior during laser peening. The effect of carbon content on mechanical properties is included in the model to expand its capability to model the carbon gradient in the carburized case. The pressure curve

generated by the vaporized plasma from the laser is used directly to drive the model. Both the accuracy of the material properties and the pressure curve are critical to the accuracy of the modeling results. Different techniques have been developed to fit the high strain rate material properties and the pressure curves from various laser peening processes [13-14]. The validated DANTE-LP database contains various aluminum alloys, Ti-6Al-4V and carburized steels with different heat treatment conditions.
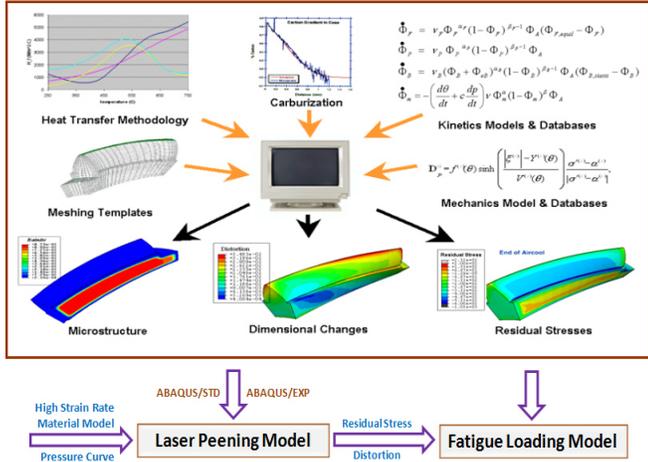

FIGURE 1 - INTEGRATED COMPUTER MODELING FOR CRABURIZATION, QUENCH HARDENING, LASER PEENING, AND FATIGUE LOADING.

The heat treatment simulation results from DANTE models include residual stresses, geometry change, and microstructural phase fractions. These predicted results are imported to the laser peening model, as shown in Figure 1. The residual stresses and carbon gradient from heat treatment are important initial conditions in the laser peening modeling. As noted, the residual stress in the final component is critical to its high cycle fatigue performance, and this can be shown by the stress states from fatigue loading models having different residual stress states resulting from different heat treatment and/or laser peening process conditions.

It is important to increase the magnitude of residual compression due to its benefit to the fatigue performance. In this paper, an innovative concept of laser peening with part preload that enhances the residual compression in the critical areas of a component is described. This concept is validated through the integrated computer modeling of quench hardening, laser peening with preload and fatigue loading processes using a carburized fatigue sample made of AISI 9310.

DESCRIPTIONS OF SELECTED SAMPLE GEOMETRY AND MATERIAL PROPERTIES

Sample Geometry and FEA Meshing

The dimensions of the sample, commonly referred to as a Hershey bar because of its shape, are shown in Figure 2. The length is 101.6mm, the width is 33.78mm, and the thickness is 8.38mm. The width of the top surface is 17.02mm. The cross section is a trapezoid as shown in Figure 2(a) to reduce the possibility of crack initiation at the edge during high cycle bending fatigue test. This Hershey sample geometry was used to study the residual stresses and fatigue performance from heat treatment and laser peening processes [15].

The finite element mesh is shown in Figure 2(b). The sample is meshed using 100% linear hexahedral elements. The total number of elements is 593,572, and the total number of nodes is 619,344. The same finite element mesh is used for carburization, quench hardening, and laser peening models. Fine elements are used in the part surface to accurately predict the gradients of carbon, temperature and stress during heat treatment, as well as the wave propagation during laser peening.
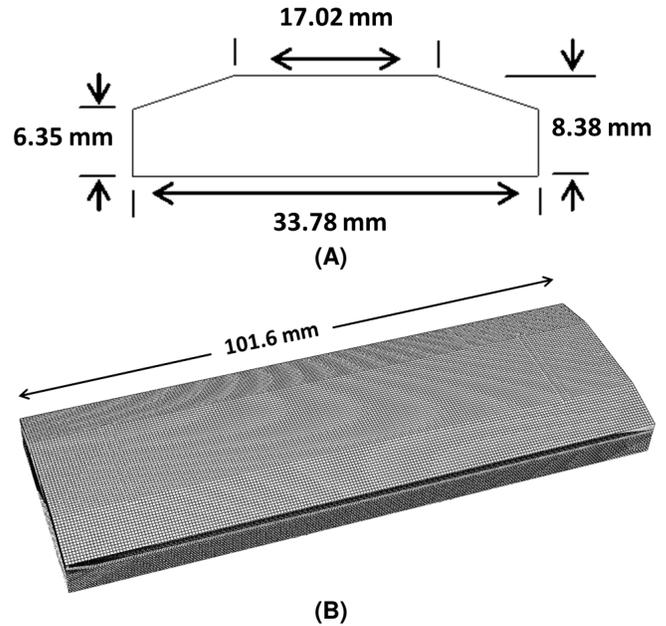

(A)

(B)

FIGURE 2 - (A) GEOMETRY, AND (B) FINITE ELEMENT MESH OF THE HERSHEY SAMPLE.

Phase Transformation Kinetics

The fatigue sample is made of AISI 9310 steel. To model the quench hardening process, models of the phase transformations are required. During quenching, the diffusive and martensitic transformation models used in DANTE are described in equations (1) and (2).

$$\frac{d\Phi_d}{dt} = \nu_d(T)\Phi_d{}^{\alpha 1}(1-\Phi_d)^{\beta 1}\Phi_a \tag{1}$$

$$\frac{d\Phi_m}{dT} = \nu_m(1-\Phi_m)^{\alpha 2}(\Phi_m + \varphi\Phi_d)^{\beta 2}\Phi_a \tag{2}$$

where Φ_d and Φ_m are the volume fractions of individual diffusive phase and martensite transformed from austenite; Φ_a is the volume fraction of austenite; ν_d and ν_m are the mobilities of tranformation; ν_d is a function of temperature, and ν_m is a constant; $\alpha 1$ and $\beta 1$ are the constants of diffusive

transformation; $\alpha2$, $\beta2$ and φ are constants of martensitic transformation. For each individual phase formation, one set of transformation kinetics parameters is required.

Figure 3(a) is a strain curve from a continuous cooling dilatometry test for AISI 9310 from DANTE database. The X-axis is temperature in Celsius, and Y-axis is length strain. Data collected during the test are temperature, length change and time. During this specific test, the cooling rate of the sample is fast enough to avoid diffusive phase formations. Starting from austentizing temperature, the dilatometry sample is fully austenitic.
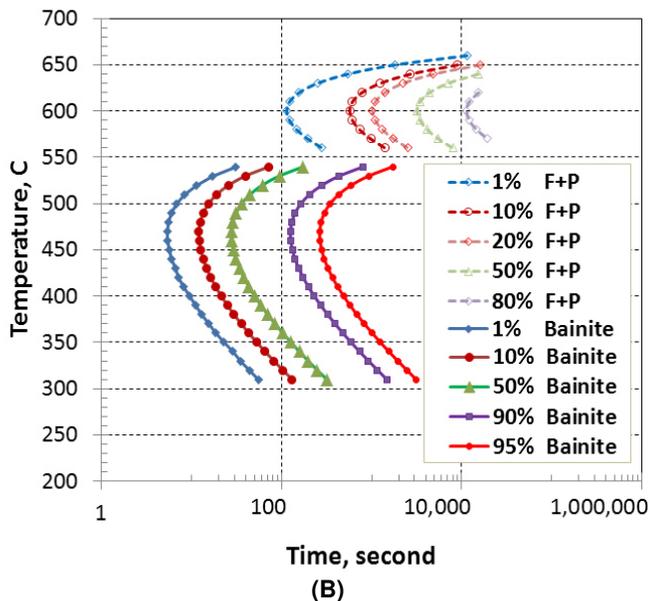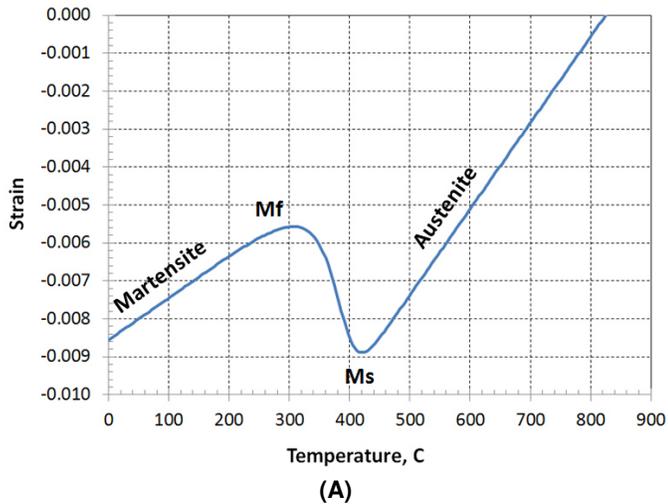

(A)

(B)

FIGURE 3 - (A) DILATOMETRY STRAIN CURVE DURING CONTINUOUS COOLING, AND (B) TTT DIAGRAMS OF AISI 9310 GENERATED FROM DANTE DATABASE.

When the sample temperature cools to the martensitic transformation starting temperature (Ms), volume expansion

begins due to the crystal strucure change from austenite's face centered cubic (FCC) lattice to martensite's body centered tetragonal (BCT) lattice. Martensite's BCT structure has a lower density than austenite's FCC structrue. The strain change during transformation is a combination of thermal strain, phase transformation volume change, and strain induced by stresses generated during the transformation. The latter strain is referred to as TRansformation Induced Plasticity or TRIP. The data obtained from this specific dilatometry test include coefficient of thermal expansion (CTE) for austenite and martensite, martensitic transformation starting and finishing temperature (Ms, Mf), transformation strain, and phase transformation kinetics (transformation rate) from austenite to martensite. These data are critical to the accuracy of modeling the internal stress and deformation caused by quenching.

Diffusive transformations are also characterized by dilatometry tests. A series of dilatometry tests with different cooling rates are required to fit a full set of diffusive and martensitic phase transformation kinetics parameters. Once the full set of phase transformation kinetics paratmeters are fit from dilatometry tests, isothermal transformation (TTT) and continuous cooling transformation (CCT) diagrams can be generated for users to review. TTT/CCT diagrams are not directly used by DANTE phase transformation kinetics models, but they are useful because users can see the hardenability of the material graphically. Figure 3(b) is an isothermal transformation diagram (TTT) for 9310 steel created from the DANTE database.

High Strain Rate Mechanical Model for Laser Peening Process

A modified Johnson-Cook model is used to describe the high strain rate stress-strain behavior with the effect of carbon variation. The modification is necessary because the carbon gradient in the carburized case from the carburization and quench hardening process. The effect of carbon on the elastic properties is negligible. In this study, Young's modulus value of 213.7 GPa is assumed for AISI 9310 tempered martensite with carbon levels from 0.1 to 0.8 wt.%. Becase there is no direct method can be used to test the high strain rate (10^6 s^{-1}) mechanical properties required for modeling the laser peening process, the properties are derived from a fitting methodology using both single shot and batch peening with characterization of surface deformation profile and residual stresses obatined from a series of LP rpocesses [14-15]. In this study, the residual stresses are measured by X-ray diffraction, and the obtained indentation profiles are measured by white light interferometer (i.e. WYKO equipment). Figure 4(a) shows calculated stress-strain curves of base carbon steel with strain rate values up to 10^6 s^{-1}. The carbon content has a significant effect on yield strength and hardening, and the fitted stress-strain curves for AISI 9380 tempered martesnite, i.e. 0.8 wt.% carbon, are shown in Figure 4(b). Tradional tension tests are done under low strain rates. Under low strain rate of 10^{-2}, the yield strength of base carbon material is about 550 MPa, and the high carbon material is up to 1100 MPa.
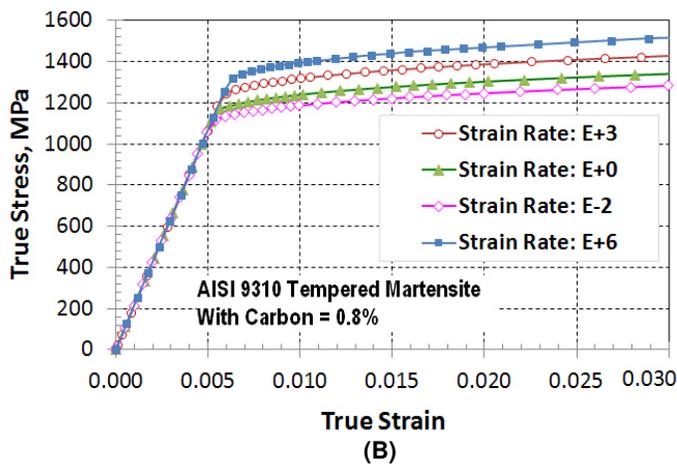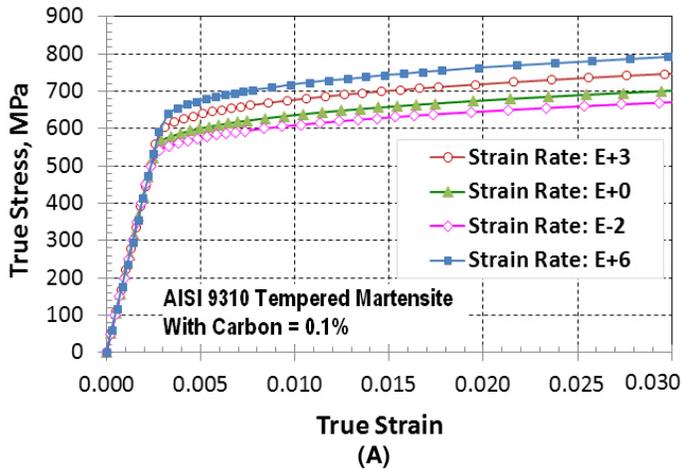
FIGURE 4 - HIGH STRAIN RATE PLASTIC PRPERTIES OF AISI 9310 (TEMPERED MARTENSITE). (A) 0.1 wt.% CARBON, AND (B) 0.8 wt.% CARBON.

HEAT TREATMENT PROCESS MODELING AND RESIDUAL STRESS VALIDATION

Brief Process Description

The Hershey sample is gas carburized, and the carburization process is described briefly below:

- Carburization temperature: 900˚ C.
- Carbon potential: 0.8 wt.%.
- Carburization time: 8 hours.

The carburization process is modeled using DANTE, and the predicted carbon distribution contour is shown in Figure 5(a). The carbon distribution in terms of depth from the surface is plotted in Figure 5(b). The effective case depth is approximately 0.8mm, using 0.4 wt.% carbon as the criterion. With a base carbon level of 0.1 wt.%, the depth of carbon penetration is over 1.5mm, which approximately doubles the effective case depth.

After carburization, the fatigue sample is quenched in oil at a temperature of 65˚ C. Because AISI 9310 has high hardenability and the sample size is relatively small, martensite

is the only phase obtained from austenite during quenching. The martensitic transformation starting temperature (Ms) decreases with the increase of carbon content. The surface carbon of the fatigue sample is 0.8 wt.%, and its Ms is about 170º C. The core of the sample has a carbon content of 0.1 wt.%, and its Ms is 425º C. Because of this difference in Ms temperatures and the lesser difference in surface and sub-surface cooling rates, the transformation to martensite under the carburized case starts and finishes earlier than in the higher carbon case. The volume expansion under the case as martensite forms plastically deforms the austenite surface. Later, the carburized surface expands due to the delayed martensitic formation, and this volume expansion creates residual compression in the carburized surface.
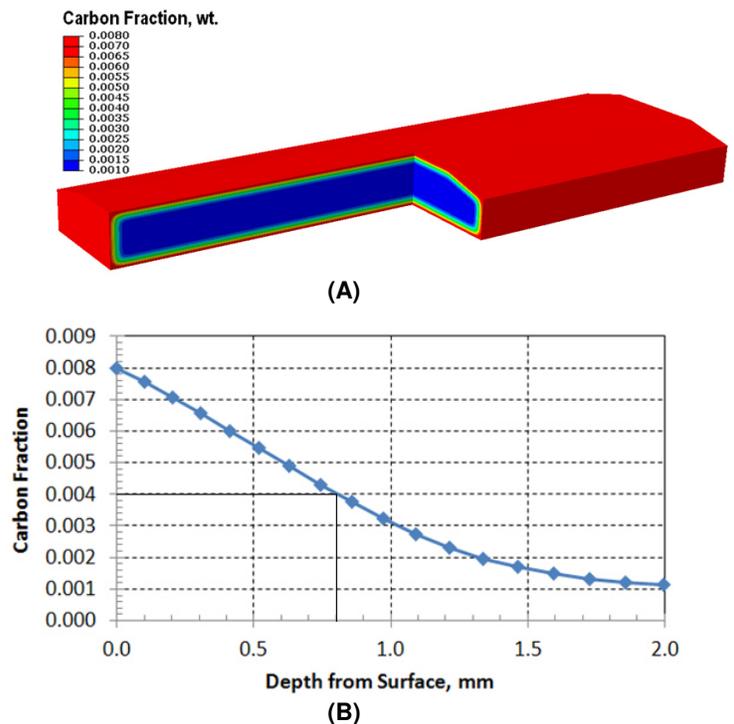

FIGURE 5 - CARBON DISTRIBUTION. (A) CONTOUR PLOT, AND (B) CURVE PLOT IN TERMS OF DEPTH.

The quenching process is modeled using DANTE. The predicted residual stress contour in the longitudinal direction is shown in Figure 6(a). The residual stresses at different locations on the surface are relatively smooth, and the magnitude of compression is approximately 300 MPa. Sub-surface tensile stresses are predicted to balance the surface compression.

X-ray diffraction is used to determine residual stresses in the longitudinal direction of quench hardened sample. The prediction and measured values in terms of depth from the top surface of the sample match closely, as shown in Figure 6(b). This work has been published in the second laser peening conference [15]. The predicted residual stress profile from heat

treatment is imported into the laser peening model, and the validation is necessary for the accuracy of integrated modeling.

(A)

(B)

FIGURE 6 - RESIDUAL STRESSES IN THE LONGITUDINAL DIRECTION AFTER QUENCHING HARDNEING. (A) CONTOUR PLOT PREDICTED BY DANTE, AND (B) COMPARISON BETWEEN DANTE PREDICTION AND X-RAY DIFFRACTION MEASUREMENT [15].

LASER PEENING PROCESS MODELING AND RESIDUAL STRESS VALIDATION

After heat treatment, the fatigue sample is laser peened. The laser peening process is modeled using DANTE-LP, which is a set of user subroutines linked to the ABAQUS solver. In a DANTE-LP model, a pressure pulse generated by the laser plasma is applied directly to the part surface. The DANTE-LP model simulates the shock wave propagation through the part. Using a laser intensity of 7GW/cm^2 and peening on Almen "C" sample made of AISI 9310 (through carburized to 0.8 wt.%) as an example, the predicted shock wave propagation through the sample is shown in Figure 7. The X-axis in Figure 7 is the distance from the peened surface, with X = 0.0mm representing the part surface. The Y-axis is the stress in the direction normal to the peened surface. The front of the shock wave shows a step at around 1900MPa stress magnitude, as indicated by the arrows in Figure 7, which indicates plastic deformation. The Hugoniot Elastic Limit (HEL) is calculated in the following equation (3):

$$\sigma_{HEL} = \frac{(1-\gamma)}{(1-2\gamma)} \sigma_Y \qquad (3)$$

where γ is poison ratio, and σ$_Y$ is the yield stress of the material. The yield stress of AISI 9310 (tempered martensite and carburized to 0.8 wt.% carbon) is approximately 1100MPa. Assuming a Poison ratio is 0.3, the calculated Hugoniot Elastic Limit using Equation (3) is 1925MPa, which matches the predicted stress magnitude range showing the plastic deformation. The predicted wave velocity is 5346 m/s, which agrees with the sound of speed in steel.
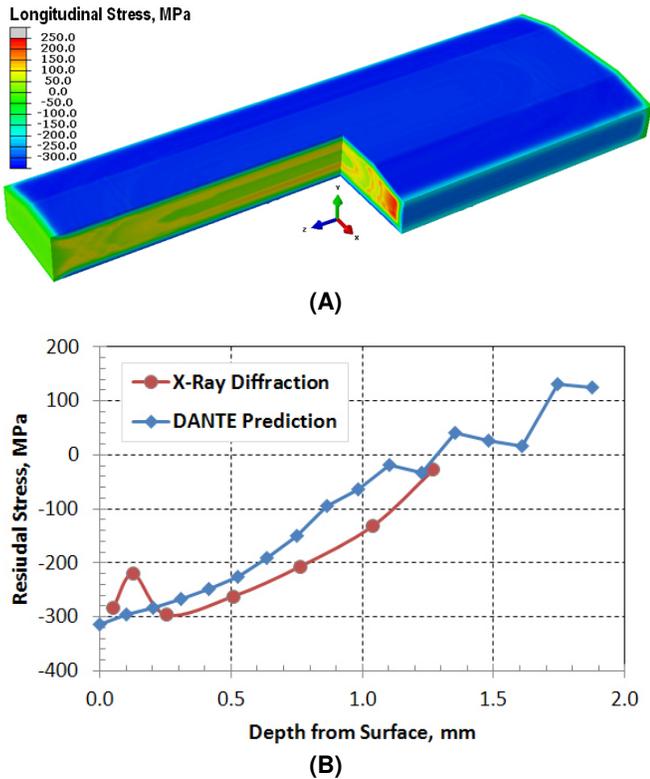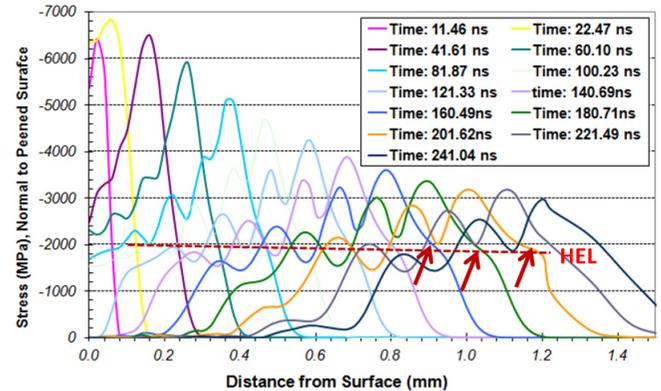

FIGURE 7 – SHOCK WAVE PROPAGATION THROUGH THE MATERIAL FROM SINGLE SHOT.

The laser intensity used to peen the fatigue sample is 7GW/cm^2, and the spot is round with a 5mm diameter. During laser peening process, one end of the sample is constrained by the fixture, and the other end is free to move as a cantilever beam. The sample is laser peened using two layers with different laser pulse duration. Each layer has 77 spots, and the peening sequence follows the transverse direction with no offset between the two layers. The predicted residual stress contour in the longitudinal direction after laser peening is shown in Figure 8(a).

During laser peening, the spatial distribution of the plastic deformation inside the laser spot is nonuniform. The residual compression inside the laser peened spot is caused by the springback and the constraint from its neighbor. The magnitude of the residual compression on the surface is not purely uniform as shown by the color difference in the contour plot. There are two main reasons for the nonuniform residual stress distribution. One reason is due to the nonuniform spatial distribution of the plastic strain inside one peened spot. The second reason is due to the peening sequence: peening of one spot changes the stress condition of its neighbor. There laser peening sequence is an important processing parameter affecting the residual stresses. A quarter of the sample is removed in Figure 8(a) to show the stresses inside the sample. Tensile residual stresses are predicted in the core of the sample to balance the surface compression.

Because the residual stress distribution is not uniform after laser peening, the predicted residual stress is averaged over a rectangular window of 2mm x 5mm as highlighted in Figure 8(a) to compare with the X-ray diffraction measurements. The size and location of the selected rectangular window match the aperture window used for residual stress measurement by X-ray diffraction. In Figure 8(b), the X-axis is the depth from the top surface of the sample, and the Y-axis represents the residual stresses in the longitudinal direction. The laser peening process 1 and process 2 in Figure 8(b) are from the same laser peening set up with different ablative layer materials (RapidCoater® and Paint). The curve labeled as "Nominal" is the average residual stress distribution from a series of processed samples and measurements. The residual stresses shown in Figure 8(b) from different laser peening processes and prediction has been published in the second laser peening conference [15]. The prediction and measurements match closely with the surface compression within the magnitude between 700 and 800 MPa.
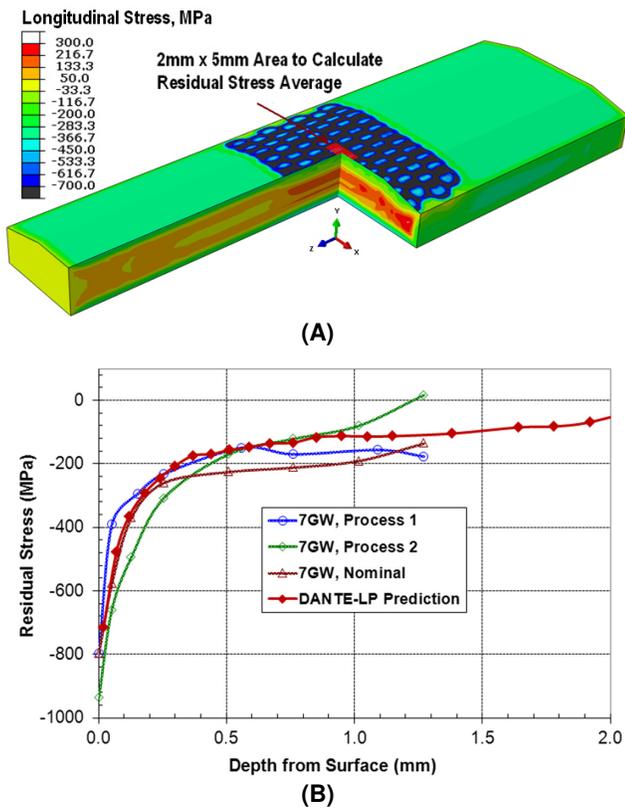

(A)

(B)

FIGURE 8 - RESIDUAL STRESSES IN THE LONGITUDINAL DIRECTION AFTER LASER PEENING. (A) CONTOUR PLOT PREDICTED BY DANTE-LP, AND (B) COMPARISON BETWEEN PREDICTION AND X-RAY DIFFRACTION MEASUREMENTS [15].

LASER PEENING PROCESS WITH PRELOAD

As mentioned in previous sections, plastic strain is required to introduce compressive residual stresses to the laser peened surface. It is easier to introduce plastic strain when the part surface is under tension prior to peening because the stress tensor of the material is closer to its yield surface. With this assumption, an innovative laser peening process with preload is invented, and this idea is validated by finite element modeling using DANTE-LP.

To introduce tensile stresses to the surface of the Hershey sample prior to laser peening, the sample is preloaded by a fixture with four pins. This preload fixture is similar to the 4-point fatigue bending set up as shown in Figure 9. The two bottom pins are constrained, and their center-to-center distance is 25.4 mm. The two pins on the top are used to apply load, and their separation distance is 76.2 mm. The total load applied to the two pins on the top is 20,000 N, with 10,000 N on each pin. With considering the residual tresses from heat treatment process, the longitudinal stress on the top surface under preload is around +550 MPa in tension, which is approximately half of its yield strength for the carburized surface. With the 4-point bending set up, the bending moment between the two inner pins is uniform, and the longitudinal stress on the peened area is also relatively uniform. The preload is modeled using ABAQUS/Standard with the assumption of the four pins being rigid surfaces.
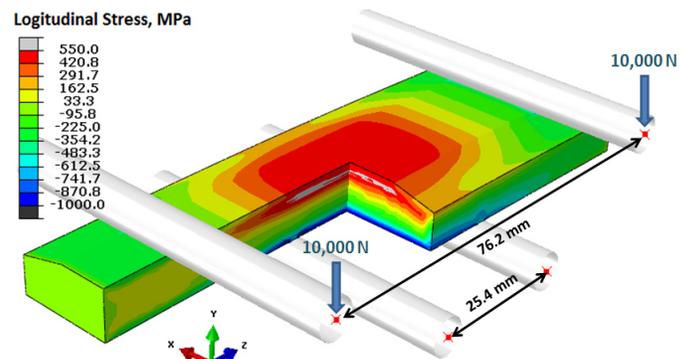

FIGURE 9 - STRESS DISTRIBUTION UNDER PRELOAD BEFORE LASER PEENING.

The preload model is similar to the loading model of the 4-point bending fatigue test. However, the real fixtures of the two applications are different. The 4-point bending fatigue test fixture is designed to take cyclic load in a fatigue test machine. The preload fixture is designed to work with laser peening equipment, and the load is applied by bending torque. Once the preload has been applied, the position of each of the four pins is locked prior to laser peening. There is a difference between locking the positions of the pins and keeping a constant load. By locking the positions of the four pins, the applied load during laser peening can be relaxed or increased due to the deformation of the sample. The process is more consistent and controllable by locking the pins instead of keeping the load constant.

The same laser peening process parameters described in the previous section are used to peen the sample under preload.

After laser peening, the sample is released from the fixture, and the predicted longitudinal residual stress contour is shown in Figure 10. The legend of stress distribution contour in Figure 10 is the same as that used in Figure 8(a). The darker color on the sample surface shown in Figure 10 indicates higher magnitude of compression generated by laser peening with preload, and the magnitude of tension in the core is also higher compared to that generated from the conventional laser peening process. The side edges also have tensile residual stresses. With this specific Hershey sample geometry, the bending stress at the side edge under 4-point bending fatigue test load is lower than that at the top surface because the side edge is closer to the mid-plane. Due to the trapezoid geometry of the sample, the cracking initiation during bending fatigue test starts on the top surface instead of the edges. In general, the laser peening on the edges of components is more difficult because of the lack of constraint from the free side. Special care of the applied laser intensity and peening sequence are required to obtain the optimum results at the edges.
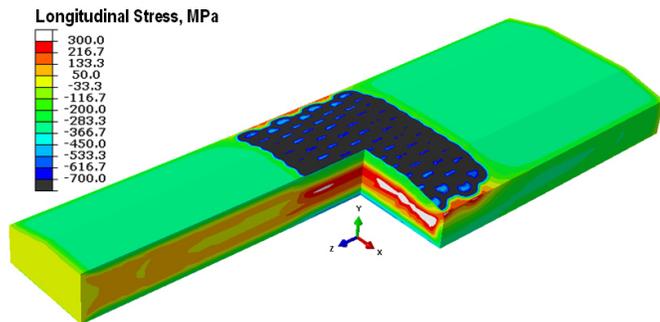

FIGURE 10 - RESIDUAL STRESSES IN THE LONGITUDINAL DIRECTION AFTER LASER PEENING WITH PRELOAD.

The predicted residual stresses from heat treatment, conventional laser peening, and laser peening with preload are compared in Figure 11. The X-axis in Figure 11 is the depth from the top surface, and the Y-axis represents the residual stresses in the longitudinal direction averaged over a 2mm x 5mm window from center of the top surface. Figure 11(a) shows the predicted stresses through the whole thickness direction, and Figure 11(b) is a zoomed in plot close to the peened surface. The surface residual stress generated from carburization and oil quench is about 300 MPa in compression. With conventional laser peening, the compression obtained is about 700 MPa. Using laser peening with preload, the surface compression is around 900 MPa. The stress variation generated by the laser peening is not compared in this study. The laser intensity and pulse duration can be optimized to improve the uniformity of residual stress distribution. The depth of compression by laser peening with preload is also deeper compared to conventional laser peening. To balance the surface compression, tensile stresses exist under the surface and in the core of the sample. Higher surface compression requires higher tension under the surface to balance. In most cases, tensile residual stresses under

the surface will not reduce the fatigue performance because the applied stress is lower and the crack initiation sites are much less relative to the surface.

The bottom surface of the sample is also carburized, and its residual stress is the same as that of the top surface after heat treatment. After conventional laser peening, the magnitude of compression on the bottom surface increases from 300 MPa to 420 MPa even the laser peening is applied on the top surface only, which is due to the bowing shape change caused by peening the top surface. The compression on the bottom surface caused by laser peening with preload is close to 500 MPa.
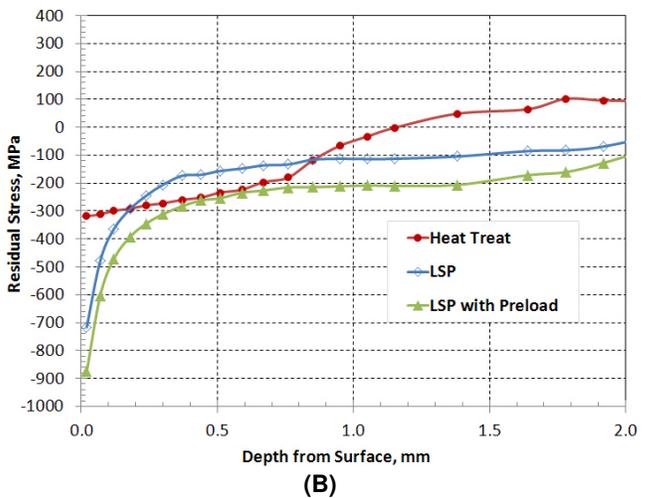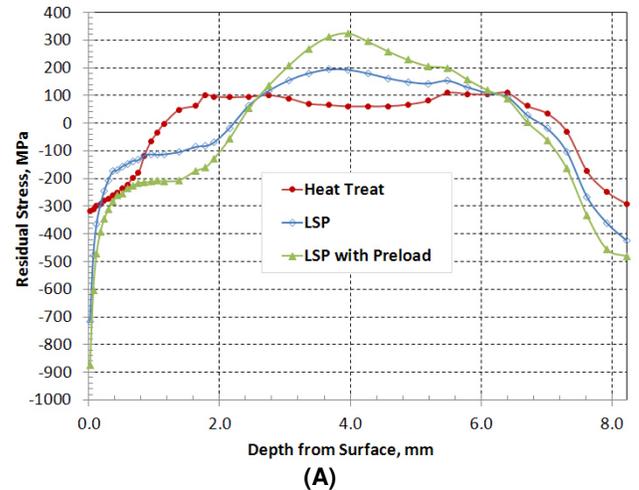

(A)

(B)

FIGURE 11 – COMPARISON OF PREDICTED RESIDUAL STRESSES. (A) THROUGH THE SAMPLE THICKNESS, AND (B) ZOOMED IN PLOT CLOSING TO SURFACE.

SUMMARY

A fatigue sample with a trapezoidal cross section and made of carburized AISI 9310 was carburized and oil quenched. The heat treatment process was modeled using DANTE, and the predicted residual stresses were validated against stresses determined from X-ray diffraction measurements. The predicted

residual stresses were imported into DANTE-LP models to predict the shock wave propagation and residual stresses generated by the laser peening process. To enhance the surface compression, an innovative laser peening process with preload was invented. With this method, the surface compression obtained was close to 900 MPa, in comparison to 700 MPa generated by conventional laser peening. The depth of the surface compression was also increased. With higher magnitude and deeper surface compression, the fatigue performance of the component is expected to be improved.

X-ray diffraction was used to validate the residual stress predictions from heat treatment and conventional laser peening process models. The invention of using preload to further improve the compressive residual stress state was investigated by using validated models to examine preload effects on stress state. In future work, the laser peening process with preload will be validated against experiments including residual stress measurements by X-ray diffraction, and high cycle fatigue test of the processed samples.

REFERENCES

[1] Sokol, D., Clauer, A., and Ravindranath, R. "Applications of Laser Peening to Titanium Alloys", ASME/JSME 2004 Pressure Vessels and Piping Division Conferecne, San Diego, CA, July 25-29, 2004.

[2] Peyre, P., Solier, A., Chaieb, I., Berthe, L., Bartnicki, E., Braham, C., and Fabbro, R., "FEM Simulation of Residual Stresses Induced by Laser Peening", The European Physical Journal Applied Physics, April 23, 2003, pp. 83-88

[3] Zhang, X., Zhang, Y., Lu, J., Xuan, F., Wang, Z., and Tu, S., "Improvement of fatigue Life of Ti-6Al-4V Alloy by Laser Shock Peening", materials Science and Engineering A, 527(2010) pp. 3411-3415

[4] James, M, Hughes, D., Chen, Z., Lombard, H., Hattingh, D., Asquith, D., Yates, J., and Webster, P., "Residual Stresses and fatigue Performance", Journal of Engineering Failure Analysis, 14(2007), pp. 384-395

[5] Shaw, B., Aylott, C., Hara, P., and Brimble, K., "The Role of Residual Stress on the fatigue Strength of High Performance Gearing", International Journal of Fatigue, 25(2003), pp. 1279-1283

[6] Obata, M., Sano, Y., Mukai, N., Yoda, M., Shima, S., and Kanno, M., "Effect of Laser Peening on Residual Stresses and Stress Corrosion Cracking for Type 304 Stainless Steel", the 7th International Conference on Shot Peening, pp. 387-394

[7] Cao, P., Liu, G., and Wu, K., "Numerical Simulation and Analysis of Heat Treatment of Large-Scale Hydraulic Steel Gate Track", International Journal of Material and Mechanical Engineering, 1(2012), pp. 16-20

[8] Natarajan, S., Muralidharan, S., and Maharaja, N., "Investigation of Significance in Phase Transformation of Power Metallurgy Steel Components during Heat Treatment – A Practical Approach", International Journal of Mechanical Engineering and technology, 4(2013), pp. 189-195

[9] Ferguson, B.L., Freborg, A.M., Li, Z., "Probe Design to Charactrize Heat Transfer during Quenching Process", Proceedings of 6th International Quenching and Control of Distortion Conference, Chicago, Illinois, September 9-13, 2012, pp. 792-801.

[10] Bammann, D., et al., "Development of a Carburizing and Quenching Simulation Tool: A Material Model for Carburizing Steels Undergoing Phase Transformations", Proceedings of the 2nd International Conference on Quenching and the Control of Distortion, November (1996), pp. 367-375.

[11] Brooks, B., and Beckermann, C., "Prediction of Heat Treatment Distortion of cast Steel C-Rings", Proceedings of the 61st SFSA Technical and Operating Conference", Steel Founders' Society of America, Chicago, IL 2007.

[12] Li, Z., Ferguson, B., and Freborg, A., "Data Needs for Modeling Heat Treatment of Steel Parts", Proceedings of Materials Science & Technology Conference, 2004, pp. 219-226.

[13] Campbell, J., Hackel, L., and Freborg, A., "LP Surface Treatment of Carburized Steels: Part I - Measured Residual Stress and Plastic Deformation", Proceedings of 1st International conference on Laser Peening, December 15-17, 2008, Houston.

[14] Li, Z., Ferguson, B., Freborg, A., Campbell, J., and Hackel, L., "Laser Peening Development for Surface Treatment of Carburized Steels: Part II – Simulation of Residual Stress and Plastic Deformation using DANTE", Proceedings of 1st International conference on Laser Peening, December 15-17, 2008, Houston.

[15] Tenaglia, R., and Li, Z., "Advances in Modeling of Laser Peening for Carburized Steels", Proceedings of 2nd International conference on Laser Peening, April 18-21, 2010, San Francisco.